⌘ *Author's Choice*

THE JOURNAL OF BIOLOGICAL CHEMISTRY VOL. 284, NO. 48, pp. 33130–33138, November 27, 2009
© 2009 by The American Society for Biochemistry and Molecular Biology, Inc. Printed in the U.S.A.

A Biosensor for Fluorescent Determination of ADP with High Time Resolution*[S]

Received for publication, July 21, 2009, and in revised form, September 17, 2009 Published, JBC Papers in Press, September 29, 2009, DOI 10.1074/jbc.M109.047118

Simone Kunzelmann and Martin R. Webb[1]

From the MRC National Institute for Medical Research, Mill Hill, London NW7 1AA, United Kingdom

Nearly every cellular process requires the presence of ATP. This is reflected in the vast number of enzymes like kinases or ATP hydrolases, both of which cleave the terminal phosphate from ATP, thereby releasing ADP. Despite the fact that ATP hydrolysis is one of the most fundamental reactions in biological systems, there are only a few methods available for direct measurements of enzymatic-driven ATP conversion. Here we describe the development of a reagentless biosensor for ADP, the common product of all ATPases and kinases, which allows the real-time detection of ADP, produced enzymatically. The biosensor is derived from a bacterial actin homologue, ParM, as protein framework. A single fluorophore (a diethylaminocoumarin), attached to ParM at the edge of the nucleotide binding site, couples ADP binding to a >3.5-fold increase in fluorescence intensity. The labeled ParM variant has high affinity for ADP (0.46 μM) and a fast signal response, controlled by the rate of ADP binding to the sensor (0.65 $\mu M^{-1}s^{-1}$). Amino acids in the active site were mutated to reduce ATP affinity and achieve a >400-fold discrimination against triphosphate binding. A further mutation ensured that the final sensor did not form filaments and, as a consequence, has extremely low ATPase activity. The broad applicability of *N*-[2-(1-maleimidyl)ethyl]-7-diethylaminocoumarin-3-carboxamide (MDCC)-ParM as a sensitive probe for ADP is demonstrated in real-time kinetic assays on two different ATPases and a protein kinase.

ATP conversion to ADP is a central process in all living organisms and is catalyzed by a vast number of different enzymes. ATP hydrolysis drives most energy-dependent cellular functions, such as metabolic processes, directed transport, force-generation, and movement. Kinases phosphorylate a wide variety of substrates from metabolic intermediates to proteins, so controlling their activity. Hence, assays to monitor the common product, ADP, have wide applications in biochemical and biomedical research ranging from a detailed understanding of mechanochemical coupling in motor proteins to screening for ATPase and kinase inhibitors. Despite the importance of ADP detection in biological systems, there are only a few methods available to date to monitor ADP, including coupled enzyme assays (1) or recognition by specific RNA (2) and antibodies (3–5).

An alternative approach is to take advantage of the highly specific interaction of the target molecule with a cognate binding protein. By attaching a fluorophore in a suitable position on the protein, ligand recognition can be coupled to an optical signal. Such fluorescent, protein-based sensors have been reported for a number of biomolecules such as sugars, amino acids, metal ions, and phosphate (6–10). This technology offers a number of advantages; the signal change can be very fast, limited only by the speed of ligand binding or the associated conformational change, and only a single component, the labeled protein, is needed for detection. Such a reagentless biosensor has been developed previously which responds to a wide range of ADP/ATP ratios (11). However, the applicability of this sensor is narrowed for the reasons that the fluorescence decreases with ADP, and this is less favorable than an increase, because the sensitivity is lower and the signal response is not linear.

Here we report the development of an ADP-specific sensor using ParM as the binding protein. ParM, an actin homologue from *Escherichia coli* involved in plasmid segregation (12, 13), was chosen as the protein scaffold for the sensor development for the following reasons. First, because of its prokaryotic origin and relatively small size, it can be strongly overexpressed in *E. coli* and, therefore, is available in large quantities. Second, crystal structures indicate that ParM undergoes a large conformation change upon ADP binding (13) that facilitates the rational design of labeling positions, where fluorophores are likely to respond to ADP binding. Third, ParM has a high affinity for ADP (14), which is advantageous for ADP detection with high sensitivity.

The ParM structure has been solved in four different states, the nucleotide-free form as well as complexes with different nucleotides (13, 15). ParM consists of two domains (I and II) that are both further divided into subdomains A and B. The nucleotide binding site is located in a cleft between the two domains with residues from both contributing to the interaction. In the absence of nucleotide, ParM is in an open conformation. The structure of the ADP complex shows a large (25°) rigid body movement of the two domains relative to each other, leading to cleft closure (Fig. 1) (13).

Although ParM has many advantageous characteristics for its development as a reagentless biosensor, there are also several properties that are potentially deleterious and need circumventing. A problem for any ADP assay is that it is likely to be performed in the presence of a large excess of ATP as substrate, which may bind and inhibit assay components. In the

* This work was supported by Medical Research Council Technology and by Medical Research Council, United Kingdom. A patent application has been made by the Medical Research Council on part of this work.

⌘ *Author's Choice*—Final version full access.

[S] The on-line version of this article (available at http://www.jbc.org) contains supplemental Tables S1–S3 and Fig. S1.

[1] To whom correspondence should be addressed: MRC National Institute for Medical Research, The Ridgeway, Mill Hill, London NW7 1AA, UK. E-mail: mwebb@nimr.mrc.ac.uk.

case of a biosensor that is based on binding ADP, discrimination against ATP binding is a necessity. A second problem is that ParM can form filaments (13), which may affect the fluorescence signal and/or nucleotide binding. Finally, ParM has low ATPase activity, which may interfere with the assay. In principle, all these potential difficulties can be addressed by manipulation of the protein, particularly by mutagenesis.

By engineering the bacterial actin ParM, we have developed a biosensor that responds to ADP binding with a large fluorescence increase, produced by a single coumarin label, MDCC.[2] The sensor has submicromolar affinity for ADP and a fast signal response. By mutating the ParM active site, we constructed a sensor variant that strongly discriminates against ATP, binding ATP >400-fold weaker than ADP. In addition, filament formation is greatly reduced in the MDCC-ParM variant, and therefore, the ATPase activity is very low. The biosensor is applied in real-time measurements of ATPase and kinase activity.

EXPERIMENTAL PROCEDURES

Plasmids—Plasmid pJSC1 for recombinant synthesis of wild-type ParM was provided by J. Löwe (MRC Laboratory of Molecular Biology, Cambridge, UK) (16). Point mutations in ParM were introduced by QuikChange site-directed mutagenesis (Stratagene) using pJSC1 as template. For all variants except those containing only the initial cysteine mutations, the ParM expression plasmid was modified so that the protein has a C-terminal hexahistidine tag for simpler and faster purification. ParM variants with a C-terminal His_6 tag were constructed by site-directed mutagenesis using the oligonucleotides 5′-GTATCTCATAGGTAATCAATCAGGATCCCATCATCATCATCATC-3′ and 5′-GATGATGGGATCCTGATTGATTACCTATGAGATACATACCG-3′. The mutagenic PCR changes the two stop codons after the ParM gene on pJSC1 to codons for Gln and Gly followed by a one-base deletion, so that the vector-encoded His_6 tag is expressed. The ParM (His_6) constructs contain the 10-amino acid extension QSGSHHHHHH at the C terminus.

Protein Expression and Purification—ParM variants were synthesized in *E. coli* BL21-AI cells (Invitrogen). ParM expression cultures were grown at 30 °C in 2×TY medium containing 100 μg of ml^{-1} ampicillin until the A_{600} was 0.4–0.6 cm^{-1}, when overexpression was induced by the addition of 2 mg $liter^{-1}$ arabinose. Cells were harvested after 16 h induction, resuspended in lysis buffer (30 mM Tris·HCl, pH 8.0, 25 mM KCl, 0.1% Triton X-100), and stored at −80 °C.

ParM (His_6) mutants were purified by nickel-chelate chromatography (for purification of ParM variants without the His_6 tag, see the Supplemental Methods). Cleared cell extracts were supplemented with 500 mM NaCl and filtered through a 0.45-μm syringe filter (Sartorius). The lysate was loaded onto a 5-ml HisTrap HP column (GE Healthcare) equilibrated with buffer A (30 mM Tris·HCl, pH 8.0, 500 mM NaCl). The column was washed with buffer A until the absorbance at 280 nm reached the base line followed by 50 ml of buffer B (30 mM Tris·HCl, pH 8.0, 25 mM KCl). ParM was eluted with a 100-ml linear gradient of 0–250 mM imidazole in buffer B adjusted to pH 8.0. Fractions containing ParM were pooled, and 10 mM dithiothreitol was added. Protein solutions were concentrated using a Vivaspin-20 centrifugal concentrator (Vivascience) before loading on a gel filtration column. Size exclusion chromatography was performed on a 120-ml HiLoad Superdex 75 column (GE Healthcare) in 30 mM Tris·HCl, pH 7.5, 25 mM KCl, and 1 mM EDTA. Proteins were concentrated in a Vivaspin-20 centrifugal concentrator (Vivascience) to 30–100 mg ml^{-1}. ParM concentrations were determined from the absorbance at 280 nm using the extinction coefficient 34,380 $M^{-1}cm^{-1}$ calculated from the primary sequence (17). Aliquots were shock-frozen in liquid nitrogen and stored at −80 °C.

Labeling of ParM with MDCC—Labeling of the final sensor variant ParM (His_6/I27C/K33A/T174A/T175N/C287A) was typically carried out on a scale of ~100 mg of protein. Labeling reactions contained 150 μM ParM and 250 μM MDCC in 30 mM Tris·HCl, pH 7.5, 25 mM KCl. The reaction mixture was incubated for 35 min and end-over-end mixing at 22 °C. 2 mM sodium 2-mercaptoethanesulfonate was added, and incubation was continued for 15 min. The solution was filtered through a 0.2-μm Acrodisc filter (Pall Corp.) and loaded onto a 5-ml HiTrap Q column (GE Healthcare) equilibrated with 30 mM Tris·HCl, pH 7.5, 25 mM KCl. The column was washed with the same buffer until the 280-nm absorbance reached base line. A 200-ml linear gradient of 25–400 mM KCl was applied. The main peak of labeled ParM, eluting at ~130 mM KCl, was pooled, and MDCC-ParM was concentrated as described above. The concentration of labeled ParM was determined using the extinction coefficients for MDCC coupled to dithiothreitol (7), $\epsilon_{430} = 46800\ M^{-1}cm^{-1}$ and $\epsilon_{280} = 7470\ M^{-1}\ cm^{-1}$, and the extinction coefficient of ParM given above. The identity of the labeled ParM variant was confirmed by electrospray-ionization mass spectrometry. The measured molecular mass was 37,214.8 Da, conforming to the theoretical mass of the ParM construct labeled with a single MDCC, 37,214.5 Da.

Nucleotides—Adenine and guanine nucleotides (Sigma) were obtained at the highest purity available. The purity of the nucleotides was analyzed by HPLC using a Partisphere-SAX column (125 × 4.5 mm, Whatman). Isocratic separation of nucleotides was performed with 0.3 M $(NH_4)_2HPO_4$, adjusted to pH 4.0 with HCl and containing 25% MeOH (v/v). The absorbance was monitored at 260 nm. Commercial ATP contained typically ~0.7% ADP. For determination of the ATP affinity of labeled ParM mutants, the ATP was further purified on a 100-ml DEAE-cellulose column using a linear gradient of 10 to 600 mM triethylammonium bicarbonate buffer pH 7.4 over 2000 ml. Fractions were analyzed by HPLC as described above. The purest fractions were pooled and rotary-evaporated to dryness under high vacuum at room temperature. ATP was washed four times with methanol by redissolving the solid in 50 ml of methanol and subsequent rotary evaporation. The dry solid was

[2] The abbreviations used are: MDCC, *N*-[2-(1-maleimidyl)ethyl]-7-diethylaminocoumarin-3-carboxamide; PBP, phosphate-binding protein; MDCC-PBP, the A197C mutant of the PBP of *E. coli* labeled with MDCC; ethenoADP, 1,N^6-ethenoadenosine 5′-diphosphate; ethenoATP, 1,N^6-ethenoadenosine 5′-triphosphate; GMPPNP, guanosine-5′-[(β,γ)imido]-triphosphate; mantADP, *N*-methyl-anthraniloyl-adenosine 5′-diphosphate; mantATP, *N*-methyl-anthraniloyl-adenosine 5′-triphosphate; HPLC, high pressure liquid chromatography.

redissolved in water and stored at −80 °C. This procedure yielded ATP, which contained <0.1% ADP, as measured by HPLC. Nucleotide concentrations were determined by absorbance measurements using the extinction coefficients ϵ_{259} = 15,400 $M^{-1}cm^{-1}$ and ϵ_{253} = 13,700 $M^{-1}cm^{-1}$ for adenine and guanine nucleotides, respectively.

Fluorescence Measurements—Fluorescence spectra, titrations, and slow kinetics were measured at 20 °C using a Cary Eclipse fluorescence spectrophotometer (Varian). Fluorescence spectra and titrations were carried out in 30 mM Tris·HCl, pH 7.5, 25 mM KCl, 3 mM $MgCl_2$, and 5 μM bovine serum albumin unless otherwise stated. MDCC fluorescence was excited at 431 nm, and emission was recorded at 474 nm. Titrations of MDCC-labeled ParM variants with adenine nucleotides were analyzed with a quadratic binding curve using Grafit software (18),

$$F = F_{min} + (F_{max} - F_{min})(K_d + P + L - ((K_d + P + L)^2 - 4PL)^{1/2})/2P \quad \text{(Eq. 1)}$$

where P and L are the total concentrations of protein and ligand, respectively, K_d is the dissociation constant, and F_{min} and F_{max} are the fluorescence intensities of the free and ligand-bound protein.

Steady-state activity measurements of PcrA helicase and PknB kinase were performed with the ADP biosensor MDCC-ParM (His_6/I27C/K33A/T174A/T175N/C287A). The helicase assay was carried out in 50 mM Tris·HCl, pH 7.5, 150 mM NaCl, 3 mM $MgCl_2$; for the kinase assay, 30 mM Tris·HCl, pH 7.5, 150 mM NaCl, 3 mM $MgCl_2$, and 2 mM dithiothreitol were used. MDCC fluorescence was measured at excitation and emission wavelengths of 431 and 474 nm, respectively. The concentrations used in the experiments are given in the respective figure legends. For calibration of the sensor response, MDCC-ParM at the concentration used in the assay was titrated with ADP, and the fluorescence was recorded. To account for the different fluorescence responses when ATP is present, these titrations were carried out at a series of different, initial ATP concentrations (see Fig. 2*D*). Thereby, the total nucleotide concentration, ATP+ADP, was held constant during the titrations, and only the ADP content was changed. This was achieved by incubating MDCC-ParM plus a particular ATP concentration in the cuvette and then titrating with an ADP solution of the same concentration as ATP in the cuvette, which also contained MDCC-ParM at the cuvette concentration. By linear regression, a gradient was obtained for each initial ATP concentration, corresponding to the change in fluorescence intensity per micromolar ADP. Instead of performing such a calibration for each initial ATP concentration used in the helicase or kinase assay, the titrations were performed at only four different total nucleotide concentrations. The calibrations for the other concentrations were then obtained by interpolation. Titrations were measured at 3, 6, 10, and 15 μM initial ATP for the PcrA assay and 10, 20, 30 and 40 μM for the PknB assay as well as in the absence of ATP. The gradients obtained in these titrations were plotted *versus* the initial ATP concentration. For each initial ATP concentration a gradient for calibration was then calculated by linear interpolation, and these were used to calculate the ADP concentrations from the fluorescence signal.

Stopped-flow Measurements—Stopped-flow experiments were carried out at 20 °C using a HiTech SF61 DX2 stopped-flow instrument equipped with a Xe/Hg lamp (TgK Scientific, UK). MDCC fluorescence was excited at 436 nm, and emission was detected with a photomultiplier after filtering scattered light through a 455-nm cut-off filter.

ADP binding kinetics of MDCC-ParM was measured in 30 mM Tris·HCl, pH 7.5, 25 mM KCl, 3 mM $MgCl_2$, and 5 μM bovine serum albumin. Association kinetics were measured under pseudo-first order conditions with at least a 10-fold excess of ADP over ParM. In displacement experiments to determine the dissociation rate constants, the preformed complex of MDCC-ParM and ADP was mixed with a 100–400-fold excess of unlabeled ParM. Single exponential curve-fitting was performed with the HiTech software.

Phosphate and ADP release kinetics during a single turnover of ATP hydrolysis by SufBC from *Thermotoga maritima* were measured with the phosphate biosensor MDCC-PBP (19) and the ADP sensor MDCC-ParM, respectively. Measurements were carried out in 50 mM Tris·HCl, pH 7.5, 100 mM KCl, 5 mM $MgCl_2$, and 2 mM dithiothreitol. A solution of 13 μM SufBC containing the respective biosensor (20 μM MDCC-PBP or 80 μM MDCC-ParM) was rapidly mixed with a 4 μM ATP solution. P_i release data were analyzed by single exponential curve-fitting using Grafit software. ADP release kinetics could be described by assuming two successive irreversible steps, where ADP is released in the second step. Curve fits were carried out with Grafit using the equation,

$$F = A(1 + (k_2/(k_1 - k_2))\exp(-k_1t) + (k_1/(k_2 - k_1))\exp(-k_2t)) + F_0 \quad \text{(Eq. 2)}$$

where F_0 is the fluorescence at time point zero, A is the total fluorescence change, and k_1 and k_2 are the rate constants of the two first order reactions.

To measure ADP dissociation kinetics from the SufBC complex, 13 μM SufBC and 4 μM ADP was preincubated in one syringe before rapidly mixing with 80 or 160 μM MDCC-ParM. Data were analyzed by single exponential curve-fitting using the HiTech software. The rate constant was only 10% different between the measurements with 80 and 160 μM MDCC-ParM.

RESULTS

Screening Mutant/Fluorophore Combinations for a Fluorescence Response to ADP—Wild-type ParM contains two cysteine residues; Cys-100 is buried in a hydrophobic core and is probably inaccessible to labeling, whereas Cys-287 (Fig. 1) is solvent-exposed and likely to be modified by cysteine-reactive fluorophores. Having shown that the latter cysteine was not useful as a fluorophore site (supplemental Table S1), it was mutated to alanine, and new cysteine residues were introduced by site-directed mutagenesis into this C287A variant. After examination of the structure of ParM and the nucleotide-induced conformation change, six different labeling positions were identified where an attached fluorophore might experience a large change in environment when ADP binds. These are

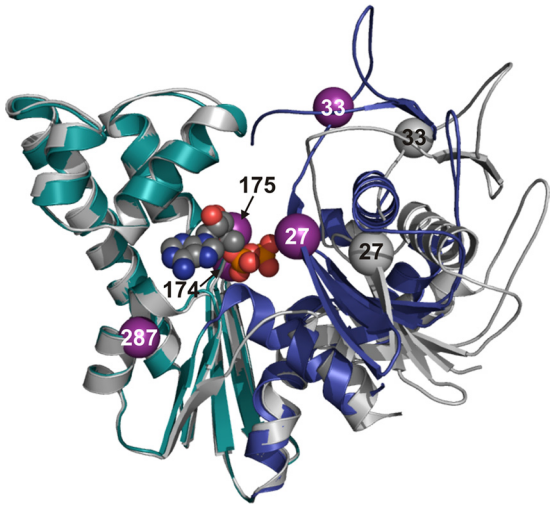

FIGURE 1. **Position of mutations in the ParM structure.** Shown is superposition of the ParM apo structure (*gray*, PDB entry 1MWM) and the ADP-bound ParM structure (subdomain I in blue and subdomain II in *cyan*, PDB entry 1MWK) showing the domain rotation upon ADP binding. The two structures were superimposed on subdomain II (residues 166–305, *cyan*). The positions of mutations in the final MDCC-ParM biosensor are shown as *purple* and *gray spheres* in the ADP bound and apo structure, respectively.

positioned on the surface, close to the ADP-triggered cleft closure. The ParM mutants, containing one reactive cysteine each, were labeled with different probes, and fluorescence spectra were recorded in the absence and presence of ADP. Only ParM (I27C/C287A) responded to ADP with an increase in fluorescence intensity, whereas all other mutants showed a less favorable signal decrease (supplemental Table S1). The largest response was obtained with the coumarin derivative, MDCC, which gave a 3-fold fluorescence increase (Fig. 2*A*). This adduct, MDCC-ParM (I27C/C287A), was chosen for further study and development.

ADP and ATP Binding Affinities—The sensitivity of ADP detection depends on both the inherent fluorescence change and ADP affinity. The ADP affinity of MDCC-ParM (I27C/C287A) was determined by titration using the fluorescence change upon ADP binding (Fig. 2*B* and Table 1). The dissociation constant, 0.31 μM, is ~8-fold lower than the value determined for ethenoADP binding to wild-type ParM (20).

A main challenge in the development of any ADP-specific biosensor that is based on binding is to achieve good discrimination against ATP. Titration of MDCC-ParM (I27C/C287A) with ATP yielded a dissociation constant of 18.7 μM, 60-fold higher than the dissociation constant of the ADP complex (Fig. 2*B* and Table 1). The size of the fluorescence change was similar to that obtained with ADP. This weaker binding of ATP was not expected, as wild-type ParM binds the fluorescent analogue ethenoATP with 60-fold higher affinity than ethenoADP (20). However, the ATP affinity relative to that of ADP is still too high for many applications, and therefore, the ParM nucleotide binding site was mutated to further increase discrimination against ATP.

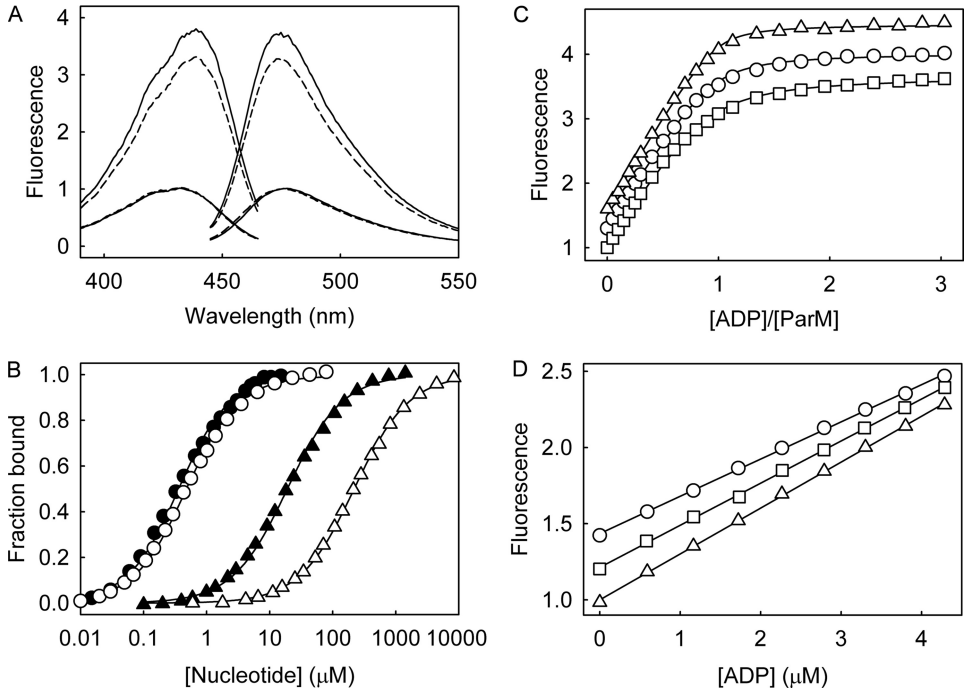

FIGURE 2. **Development of the MDCC-ParM based ADP sensor.** *A*, shown are fluorescence excitation and emission spectra of 1 μM MDCC-ParM (I27C/C287A) (*dashed lines*) and 1 μM MDCC-ParM (His_6/I27C/K33A/T174A/T175N/C287A) (*solid lines*) in the absence of ADP (lower intensity) and in the presence of 200 μM ADP (high intensity). Spectra were recorded at excitation and emission wavelength of 436 and 474 nm, respectively, with 5 nm slit width. *B*, shown is titration of MDCC-ParM (I27C/C287A) (*solid symbols*) and MDCC-ParM (His_6/I27C/K33A/T174A/T175N/C287A) (*open symbols*), both at a concentration of 0.1 μM, with ADP (*circles*) and ATP (*triangles*). Data were analyzed using a quadratic binding curve (Equation 1 under "Experimental Procedures"). The dissociation constants obtained from these fits are shown in Table 1. *C*, active site titrations are shown of 5 μM (*squares*), 10 μM (*circles*), and 20 μM (*triangles*) MDCC-ParM (His_6/I27C/K33A/T174A/T175N/C287A) with ADP. Curve-fitting was performed as in *B*, but K_d was fixed to the value obtained in *B*, and only the ParM concentration was allowed to vary. The results for the active site concentrations were 4.5, 9.7, and 19.8 μM. *D*, shown is a comparison of the fluorescence response in the absence and presence of ATP. 10 μM MDCC-ParM-only (*triangles*) and MDCC-ParM plus 20 μM ATP (*squares*) or 40 μM ATP (*circles*) were titrated with ADP. In the last two experiments the total nucleotide concentration, [ATP]+[ADP], was held constant at 20 or 40 μM, and only the proportion of ADP was changed. The fluorescence response was linear with slopes of 0.305, 0.283, and 0.252 μM^{-1} at 0, 20, and 40 μM ATP, respectively.

Mutations to Enhance Selectivity for ADP Versus ATP—The crystal structures of ParM in complex with ADP (13) and the non-hydrolyzable GTP analogue GMPPNP (15) indicate a very similar conformation of the protein in the diphosphate and triphosphate states. Examination of these structures suggested mutations that might weaken ATP binding without changing the ADP affinity. First, the side chains of Ser-9, Thr-174, and Thr-175 form hydrogen bonds to the γ-phosphate of GMPPNP (15) but are not within hydrogen-bonding distance of the ADP (13). Removing these hydroxyl side chains by mutation to alanine might, therefore, selectively weaken triphosphate binding. The second

TABLE 1

Dissociation constants and fluorescence changes for binding of ADP and ATP to MDCC-ParM mutants at different stages of the sensor development

The fluorescence change upon ADP and ATP binding (F_+/F_-) and the dissociation constants (K_d) were obtained from fluorescence titrations at 20 °C in 30 mM Tris·HCl buffer, pH 7.5, 25 mM KCl, 3 mM $MgCl_2$, and 5 μM BSA. ATP titrations were performed with highly purified ATP containing <0.1% ADP. All ParM variants except the initial double mutant I27C/C287A additionally contain a C-terminal His_6 tag. In four different batches of labeled ParM (His_6/I27C/K33A/T174A/T175N/C287A) the ADP affinity varied between 0.38 and 0.52 μM, and the signal change was between 3.3- and 4.1-fold.

ParM mutant	ADP		ATP		K_d ratio, ATP/ADP
	F_{+ADP}/F_{-ADP}	K_d	F_{+ADP}/F_{-ADP}	K_d	
		μM		μM	
I27C/C287A	3.0	0.31	3.1	18.7	60
I27C/T174A/T175N/C287A	3.5	0.51	3.3	203	398
I27C/K33A/T174A/T175N/C287A	3.5	0.46	3.2	212	460

approach was to block the γ-phosphate binding site by introducing more bulky amino acids at positions 9, 148, and 175. On the background of ParM (His_6/I27C/C287A), 10 different active site mutant proteins were generated, labeled with MDCC, and analyzed for ADP and ATP binding affinity (supplemental Table S2). The best combination of active site mutations in terms of selectivity for ADP was T174A/T175N; this mutant bound ATP ~400-fold weaker than ADP while retaining tight affinity for ADP and a large fluorescence enhancement (Table 1). This construct, ParM (His_6/I27C/T174A/T175N/C287A), was used for further experiments.

Mutations to Inhibit Filament Formation—Wild-type ParM forms actin-like filaments, which are essential for its function in plasmid segregation (21) but could disturb the sensor function of ParM. Filament formation may interfere with the fluorescence signal, and the ATPase activity of ParM is strongly enhanced in the filament (20, 21). The polymerization of MDCC-ParM (His_6/I27C/T174A/T175N/C287A) was investigated using light scattering. At 10–40 μM, this variant formed filaments when ATP was added but not with ADP or in the absence of nucleotide (supplemental Fig. S1*A*). The nucleation and polymerization kinetics were much slower than for wild-type ParM, but the critical concentration, 2.5 μM, was very similar to wild-type ParM (20). Therefore, further mutations were introduced to block filament formation. Among others, the two point mutations K33A and R34A have been shown to inhibit filament formation (16), and these residues participate in interactions between protomers in a model of the ParM filament (15). We have introduced each mutation into ParM (His_6/I27C/T174A/T175N/C287A) and analyzed the labeled proteins for polymerization. Light scattering assays showed that the K33A mutation blocks filament formation more efficiently; no increase in light scattering was detected over a period of 4 h even at very high (120 μM) concentrations of the sensor (supplemental Fig. S1*B*). Thus, the ParM variant containing the K33A mutation, MDCC-ParM (His_6/I27C/K33A/T174A/T175N/C287A), was chosen as the final ADP biosensor, hereafter referred to as MDCC-ParM.

As mentioned above, filament formation is related to an acceleration of ATP hydrolysis, and therefore, the K33A mutation is expected to decrease ATPase activity. The ATPase rate of MDCC-ParM was measured using a phosphate biosensor, rhodamine-PBP (adduct of the A17C/A197C double mutant of *E. coli* phosphate-binding protein with two molecules of 6-iodoacetamidotetramethylrhodamine) (22) (data not shown). ATP hydrolysis was very slow, with a rate constant of $<0.001\ min^{-1}$, which is >10-fold lower than MDCC-ParM without the K33A mutation. Thus, the K33A mutation not only blocks filament formation but thereby also inhibits ATPase activity.

Characterization of the Final ADP Sensor, MDCC-ParM—Titrations of MDCC-ParM with ADP and ATP showed that the K33A mutation did not alter ADP affinity and discrimination against ATP (Fig. 2*B* and Table 1). Thus, the final sensor retains submicromolar ADP sensitivity and high selectivity for the diphosphate. Although all data described so far were obtained in buffer containing low salt concentrations (25 mM KCl), the influence of physiological ionic strength was tested using 150 mM KCl or NaCl (supplemental Table S3). The fluorescence response to ADP did not significantly vary, but there were small changes (maximal 3-fold) in nucleotide affinity. However, the ADP affinity was significantly lower (4.1 μM) in the absence of KCl or NaCl (supplemental Table S3).

Accurate measurement of ADP concentrations using MDCC-ParM requires calibration of the fluorescence signal under the same conditions. Active site titrations of MDCC-ParM showed a linear fluorescence increase up to at least half-saturation of the sensor (Fig. 2*C*). At 20 μM MDCC-ParM, the fluorescence change is 3.8-fold, and the concentration of active sites is 19.8 μM, in very good agreement with the concentration determined from its absorbance spectrum. In most applications of the sensor, ADP is likely to be measured as a product from ATP substrate, and therefore ATP will be present in the assay solutions. Therefore, calibration curves were determined in the presence of different ATP concentrations but at constant total nucleotide concentration, ATP+ADP (Fig. 2*D*). A linear relationship between fluorescence intensity and ADP concentration was observed, but the slope decreased with increasing concentrations of ATP.

To assess the suitability of MDCC-ParM for real-time measurements, the kinetics of ADP binding and dissociation were investigated in stopped-flow experiments. A single exponential increase in fluorescence was observed after mixing MDCC-ParM and ADP (Fig. 3*A*). The observed rate constants showed a linear dependence on ADP concentrations, and the slope gave the association rate constant, $0.65\ \mu M^{-1}s^{-1}$. This linear dependence indicates that the rate of the signal response is controlled by ADP binding and not by a conformational change. The dissociation rate constant was measured by displacement experiments starting from a complex of MDCC-ParM·ADP and trapping dissociated ADP with a large excess of unlabeled

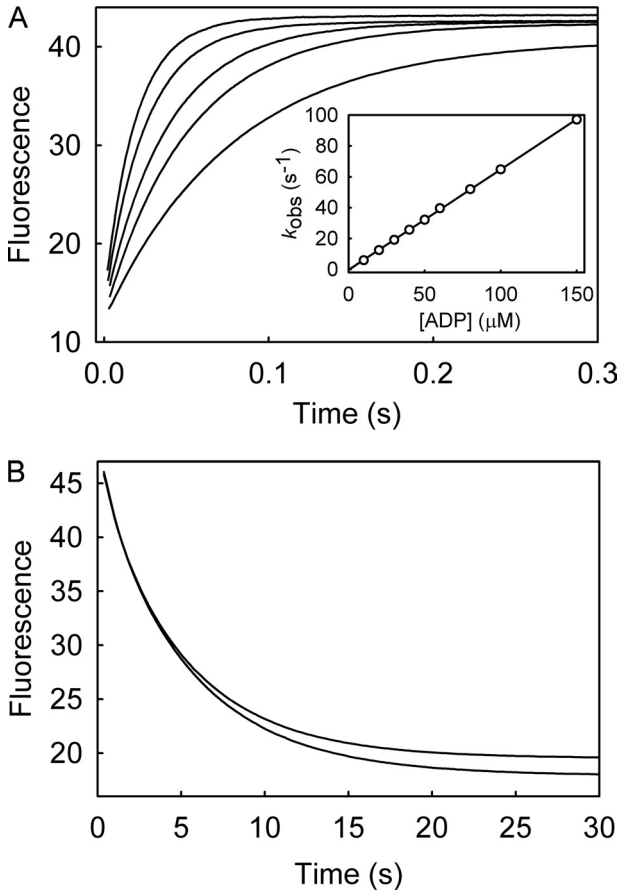

FIGURE 3. **Association and dissociation kinetics of ADP with MDCC-ParM.** *A*, association kinetics were measured under pseudo-first order conditions by mixing MDCC-ParM with ADP in a stopped-flow apparatus. Time courses of fluorescence change upon ADP binding to 0.25 μM MDCC-ParM are shown at different ADP concentrations (20, 30, 40, 50, 60, and 80 μM). The time courses shown are the average of three individual stopped-flow traces. Data are well described by single exponential curves yielding the observed rate constants, k_{obs}. *Inset*, a secondary plot of the observed rate constants *versus* ADP concentration is shown. The association rate constant, 0.65 $\pm$ 0.01 $\mu M^{-1}s^{-1}$, was obtained from the slope of a linear regression analysis. *B*, shown are dissociation kinetics of ADP from MDCC-ParM. The preformed complex of MDCC-ParM and ADP (0.5 and 2 μM) was mixed in the stopped-flow with 100 μM (*upper trace)* or 200 μM (*lower trace*) of unlabeled ParM mutant. Three individual traces were averaged to obtain the time courses shown. The rate constants determined from single exponential fits to the experimental data with 100 and 200 μM displacer are 0.20 $\pm$ 0.01 and 0.18 $\pm$ 0.01 s^{-1}, respectively.

ParM (Fig. 3*B*). A value of 0.19 s^{-1} was obtained, yielding the dissociation constant 0.30 μM, in good agreement with data from equilibrium titrations (Table 1).

Prokaryotic and archeabacterial homologues of actin, including ParM, MreB, FtsA, and Ta0583, show a rather low specificity for the base (23–25). In addition to adenine nucleotides, ParM has been reported to bind the guanine nucleotides GDP and GTP (15), but the binding affinity was not determined. The addition of GDP to MDCC-ParM resulted in only a small, 1.2-fold, increase in fluorescence (data not shown). However, competitive titrations showed that GDP can displace ADP from MDCC-ParM, and the dissociation constant for GDP, 4.4 μM, was only 10-fold higher than that for ADP (data not shown). In conclusion, GDP binds to the sensor but does not induce a large change in MDCC fluorescence. GDP competes with ADP for the MDCC-ParM binding site and, therefore, its presence might interfere with ADP detection.

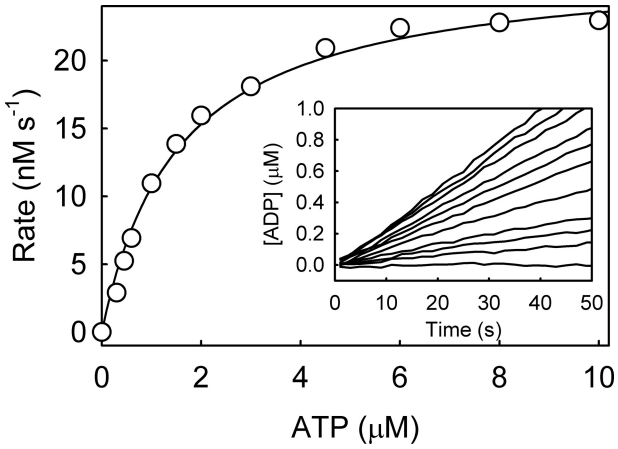

FIGURE 4. **ATP hydrolysis by PcrA helicase during translocation along single stranded DNA.** ADP generation of PcrA when translocating along single-stranded DNA was monitored using the ADP sensor MDCC-ParM. 5 μM MDCC-ParM, 0.5 μM dT_{20}, and different concentrations of ATP were preincubated in the cuvette, and the reaction was started by the addition of 2 nM PcrA. ADP concentrations were calculated from the fluorescence signal using the calibration method described under "Experimental Procedures." Time courses of ADP generation at different ATP concentrations (from *bottom* to *top*, 0, 0.3, 0.45, 0.6, 1, 1.5, 2, 3, 4.5, 8, and 15 μM) are in the *inset*. The initial rates were determined by linear regression to data points below 10% ATP turnover and plotted *versus* ATP concentration. The parameters K_m, 1.6 μM, and k_{cat}, 13.7 s^{-1} were obtained from a curve fit according to the Michaelis-Menten equation.

Steady-state Measurements of ATPase and Kinase Activity—A DNA helicase, PcrA, was used as an ATPase system to demonstrate application of MDCC-ParM in a real-time assay. PcrA, from *Bacillus stearothermophilus*, is involved in plasmid replication (26) and moves rapidly along short single-stranded oligonucleotides, hydrolyzing one ATP per base translocated (27, 28). In a steady-state assay, the hydrolysis rate of PcrA was measured in the presence of a short oligonucleotide (dT_{20}) using the MDCC-ParM biosensor. The kinetics of ADP generation was monitored at different ATP concentrations (Fig. 4). A set of calibration curves, which accounts for different fluorescence responses at different ATP concentrations, was used to calculate the ADP concentrations from the fluorescence signal (see "Experimental Procedures"). A plot of the initial rates *versus* ATP concentration gave K_m as 1.6 μM and k_{cat} as 13.7 s^{-1} (Fig. 4). However, very similar results were obtained when a single calibration was used for all the measurements at different ATP concentrations. In this case the Michaelis-Menten constant is calculated as 1.4 μM (17% lower). Using the calibration at 15 μM total nucleotide concentration (the maximum ATP used), k_{cat} was calculated as 14.0 s^{-1} (2% higher). Alternatively, using the calibration in the absence of ATP yielded a k_{cat} of 12.2 s^{-1} (11% lower). For comparison, the experiment was repeated under the same conditions but using the well characterized phosphate biosensor, MDCC-PBP (19) (data not shown). The parameters obtained were K_m 1.7 μM and k_{cat} 11.5 s^{-1}, supporting the results from the experiments using the ADP biosensor MDCC-ParM.

The protein kinase PknB from *Mycobacterium tuberculosis* was used as a second example of applying the ADP biosensor. PknB is a Ser/Thr kinase essential for mycobacterial growth (29). A recently identified substrate of PknB is the FHA (Forkhead-associated) domain of Rv1827 (30), which is involved in regulation of glutamate metabolism (31). The steady-state

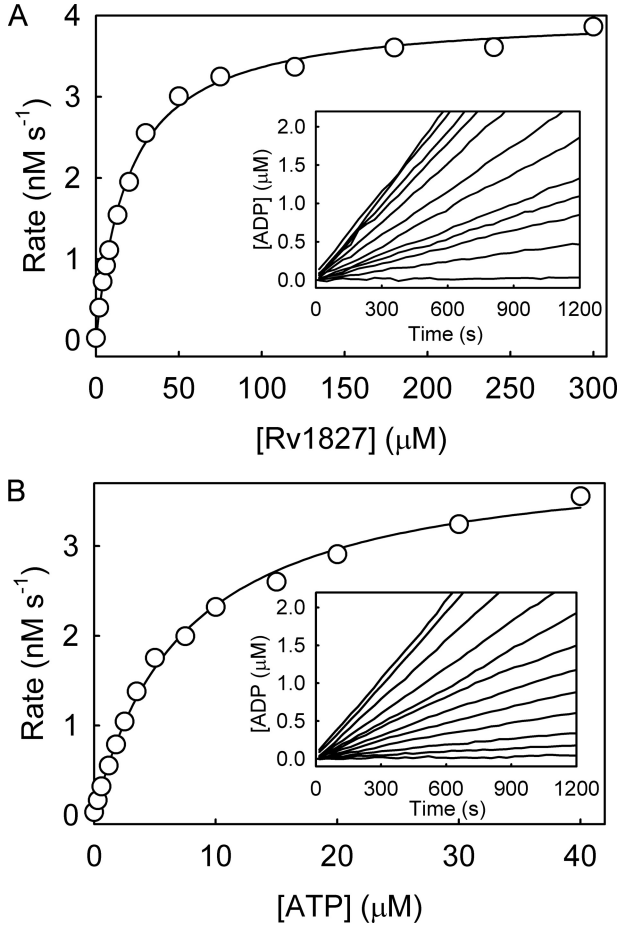

FIGURE 5. **Phosphorylation of Rv1827 by the protein kinase PknB.** Phosphorylation of Rv1827 by the protein kinase PknB was measured using the MDCC-ParM biosensor to monitor the kinetics of ADP generation. The experiments were carried out as described for the helicase assay with 50 nM PknB, 10 μM MDCC-ParM, and constant 40 μM ATP or 300 μM Rv1827, varying the concentration of the second substrate Rv1827 or ATP. *A*, a plot of initial rates against the concentration of Rv1827 is shown. Data were analyzed according to the Michaelis-Menten equation, yielding K_m^{Rv1827} 20 μM and k_{cat} 4.7 min^{-1}. *Inset*, time courses of ADP generation during phosphorylation of Rv1827 by PknB measured at different concentrations of the protein substrate Rv1827 (from *bottom* to *top*, 0, 2, 4, 6, 8, 13, 20, 30, 50, 75, 180, and 300 μM). *B*, shown is a plot of initial rates against the concentration of ATP. Curve-fitting results in the Michaelis-Menten parameters K_m^{ATP} 7.5 μM and k_{cat} 4.9 min^{-1}. *Inset*, time courses of ADP generation measured at different concentrations of the ATP (from *bottom* to *top*, 0, 0.3, 0.6, 1.2, 1.8, 2.5, 3.5, 5, 7.5, 15, 30, and 40 μM).

kinetics of Rv1827 phosphorylation by the PknB kinase domain ($PknB^{1-279}$) was monitored by following the accompanying ADP generation with the biosensor MDCC-ParM (Fig. 5). The Michaelis-Menten parameters of both substrates were determined. For the protein substrate Rv1827 the values K_m 20 μM and k_{cat} 4.7 min^{-1} were obtained (Fig. 5*A*). The results from data at different initial ATP concentrations were K_m 7.5 μM and k_{cat}, 4.9 min^{-1} (Fig. 5*B*).

P_i and ADP Release during ATP Hydrolysis of SufBC—SufC is an ATPase involved in Fe-S cluster assembly under stress conditions (32, 33). SufC and the associated protein SufB are found in bacteria, including human pathogens (*e.g. Yersinia pestis*, *M. tuberculosis*), Archaea, and the plastid organelle of algae and plants (32). The kinetic mechanism of the SufBC complex has been studied using fluorescent nucleotide analogues mantATP and mantADP (34, 35). Here, both the ADP

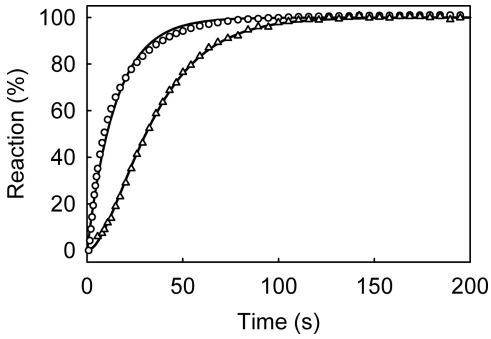

FIGURE 6. **Phosphate and ADP release during a single turnover of ATP hydrolysis by SufBC.** Phosphate release (*circles*) and ADP release (*triangles*) were measured using the biosensors MDCC-PBP and MDCC-ParM, respectively. In a stopped-flow apparatus 13 μM SufBC and either 20 μM MDCC-PBP or 80 μM MDCC-ParM were mixed with 4 μM ATP, and the fluorescence was recorded. Data represent the averages of three individual stopped-flow traces. Single exponential curve-fitting to the phosphate release data (*solid line*) gives a rate constant of 0.066 $\pm$ 0.001 s^{-1}. ADP release data were analyzed using a double exponential function (*solid line*), assuming a reaction sequence of two irreversible steps, where ADP is released in the second step. This results in the first order rate constants of the two steps, 0.058 $\pm$ 0.001 s^{-1} and 0.050 $\pm$ 0.002 s^{-1}.

biosensor (MDCC-ParM) and a P_i biosensor (MDCC-PBP (19)) were used to study ADP and P_i release during a single turnover of ATP hydrolysis by SufBC (Fig. 6). P_i is released first at 0.070 s^{-1}, most likely controlled by ATP cleavage, as the rate constant is very similar to that of mantATP cleavage (34). The fluorescence trace of MDCC-ParM showed a marked lag phase, characterized by a very similar rate constant to P_i release, 0.058 s^{-1}, before ADP dissociation occurs at 0.050 s^{-1}, comparable with the mantADP dissociation rate constant 0.038 s^{-1} (34). Direct dissociation of ADP from the SufBC complex was also measured by mixing the preincubated SufBC·ADP complex with MDCC-ParM (data not shown). Fluorescence traces were single exponentials with a rate constant of 0.046 s^{-1}, conforming to the rate constant of ADP release during ATP hydrolysis. These measurements with unlabeled ATP and ADP confirm the studies using mant nucleotides (34), indicating that the mant group does not have a large effect on the SufBC/nucleotide interactions.

DISCUSSION

In the present study we have described an ADP biosensor which is based on an engineered bacterial actin homologue, ParM, labeled with a single coumarin fluorophore, MDCC. The MDCC is positioned on the β-sheet of domain I and brought close to domain II upon ADP-triggered cleft closure (Fig. 1) (13). The large fluorescence change is likely to originate from the interaction of the fluorophore with the second subdomain, thus reporting the conformational change. However, because the labeling position is close to the nucleotide base (Fig. 1), a direct interaction of the MDCC with ADP might also contribute to the observed signal change. The lack of a fluorescence signal with GDP might imply a specific interaction of the MDCC-fluorophore with the adenine base.

As outlined in the introduction, a major challenge in the development of an ADP sensor is to achieve discrimination against ATP. Wild-type ParM binds the triphosphate analogue ethenoATP 60-fold tighter than ethenoADP (20). In contrast,

the first sensor variant, MDCC-labeled ParM (I27C/C287A), has 60-fold binding preference for ADP over ATP. This surprisingly large difference might be caused by the two point mutations, by the MDCC label, or by the use of the etheno analogues. The discrimination against ATP was further improved by two additional mutations in the active site, T174A and T175N, so the final sensor MDCC-ParM binds ATP >400-fold weaker than ADP with a dissociation constant of ~200 μM. Introducing an additional single point mutation, K33A, abolished filament formation under all conditions tested and reduced the ATPase activity to a very low level, $<0.001\ min^{-1}$ at 20 °C.

The ParM-based ADP biosensor can be used for determination of ADP *in vitro* and is especially well suited for time-resolved ADP assays to investigate kinases and ATPases. The characterization of the biosensor and the examples of its applications in ATPase and kinase assays bring out the advantages and limitation of MDCC-ParM as a probe for ADP generation. The strong ADP binding affinity of MDCC-ParM enables the biosensor to detect ADP with high sensitivity. By applying the sensor at >5 μM, 10-fold above the K_d value, a linear dependence of the fluorescence on ADP concentration was obtained. Thus, MDCC-ParM was used in stoichiometric amounts, detecting every molecule of ADP generated, and is, therefore, likely to be useful for detection of ADP in the range of submicromolar to ~10 μM.

Although MDCC-ParM has high (>400-fold) selectivity for ADP *versus* ATP, similar or even higher than the sensors based on RNA (2) and antibody recognition (3–5), the dissociation constant for ATP binding of 200 μM still sets a limit on ATP. At high ATP concentrations sensitivity is lost due to ATP binding to the sensor. However, for this type of sensitive assay, ADP contamination in the ATP may become a significant factor in limiting the ATP concentration range regardless of which ADP-detecting assay system is used. Commercial ATP, at the highest purity available, contains 0.1–1% ADP even before storing, therefore increasing background fluorescence. Careful purification can take this to <0.1% for non-routine use.

The MDCC-ParM sensor provides several advantages in comparison to the current ADP assays mentioned in the Introduction. First, the MDCC-ParM biosensor can detect ADP with submicromolar sensitivity with a linear signal response because of its high ADP affinity and the large fluorescence increase. Second, MDCC-ParM is a one-component system where only the labeled protein is required for the assay. There is a requirement for magnesium ions, but normally Mg^{2+} would also be necessary for the ATPase or kinase reaction being studied. Thus, the assay is simple, and the likelihood of interference with other assay components, such as buffers, ions, cofactors, and enzyme inhibitors, is relatively low. This might be particularly important for screening assays, where a large number of compounds are tested.

A third major advantage of MDCC-ParM over other ADP sensor systems is speed; most recent ADP detection systems, *e.g.* the coupled enzyme assay (1), the Riboreporter assay (2), and also antibody-based detection methods (3–5), have been developed specifically for high-throughput screening formats, where a short response time is not a major requirement, and indeed, these systems react relatively slowly. Although these methods, apart from the Riboreporter assay, can be used for real-time monitoring of ADP generation, measurements are limited to a time scale of minutes. An inherent problem of coupled-enzyme assays, such as the most widely used pyruvate kinase/lactate dehydrogenase assay, is the occurrence of lag phases, depending on the concentrations used that can lead to misinterpretation or artifacts. None of the methods described is particularly suitable for transient kinetic investigations. The only protein-based ADP sensor described so far shows a faster response (11), and this biosensor has been used in transient kinetic experiments (36), although high ATP or ADP concentrations are needed for a fast response. In contrast, for MDCC-ParM in excess over the ADP, the response rate will depend on the MDCC-ParM concentration and, thus, will be constant over a range of ATP concentrations. As shown in Fig. 3*A*, MDCC-ParM at very high concentrations can respond to ADP concentration changes with rate constants of $>100\ s^{-1}$. However, there is a compromise between speed, sensitivity, and protein consumption when high concentrations of MDCC-ParM are used. With an association rate constant of 0.65 $\mu M^{-1}s^{-1}$, in routine use of the assay at up to 20 μM protein, there is a limit due to the response of $\sim 13\ s^{-1}$ at 20 °C.

Many studies on ATPases and kinases rely on the use of fluorescently labeled nucleotides, in particular when kinetic mechanisms are investigated and high time-resolution is required. The fluorescent labels are often relatively large in comparison to the nucleotides and can strongly affect the affinity and dynamics of the protein/nucleotide interaction. In contrast, the ADP biosensor has the important advantage that measurements are performed with the physiological ligands ATP and ADP. The MDCC-ParM biosensor represents a simple, sensitive, and direct method to measure ADP concentration changes in real time, in particular to assay ATPase and kinase activity. Thus, it provides a generic method to study this large variety of biological important reactions.

Acknowledgments—We thank Dr. S. Howell (National Institute for Medical Research (NIMR)) for recording the mass spectra, Dr. J. Salje and Dr. J. Löwe (MRC Laboratory of Molecular Biology, Cambridge, UK) for providing the plasmid pJSC1 for ParM expression, Dr. T. J. Nott (NIMR) for the gift of purified PknB kinase domain and Rv1827 protein, Dr. K. Rangachari (NIMR) for the gift of purified SufBC complex, Dr. A. Slatter (NIMR) for the purified PcrA, G. Reid (NIMR) for purification of the ATP, and J. Hunter (NIMR) for preparing the rhodamine- and MDCC-PBP.

REFERENCES

1. Charter, N. W., Kauffman, L., Singh, R., and Eglen, R. M. (2006) *J. Biomol. Screen.* **11,** 390–399
2. Srinivasan, J., Cload, S. T., Hamaguchi, N., Kurz, J., Keene, S., Kurz, M., Boomer, R. M., Blanchard, J., Epstein, D., Wilson, C., and Diener, J. L. (2004) *Chem. Biol.* **11,** 499–508
3. Kleman-Leyer, K. M., Klink, T. A., Kopp, A. L., Westermeyer, T. A., Koeff, M. D., Larson, B. R., Worzella, T. J., Pinchard, C. A., van de Kar, S. A., Zaman, G. J., Hornberg, J. J., and Lowery, R. G. (2009) *Assay Drug Dev. Technol.* **7,** 56–67
4. Hong, L., Quinn, C. M., and Jia, Y. (2009) *Anal. Biochem.* **391,** 31–38
5. Lowery, R. G., and Kleman-Leyer, K. (2006) *Expert Opin. Ther. Targets* **10,** 179–190

6. Gilardi, G., Zhou, L. Q., Hibbert, L., and Cass, A. E. G. (1994) *Anal. Chem.* **66,** 3840–3847
7. Brune, M., Hunter, J. L., Corrie, J. E., and Webb, M. R. (1994) *Biochemistry* **33,** 8262–8271
8. Salins, L. L., Ware, R. A., Ensor, C. M., and Daunert, S. (2001) *Anal. Biochem.* **294,** 19–26
9. Dattelbaum, J. D., and Lakowicz, J. R. (2001) *Anal. Biochem.* **291,** 89–95
10. de Lorimier, R. M., Smith, J. J., Dwyer, M. A., Looger, L. L., Sali, K. M., Paavola, C. D., Rizk, S. S., Sadigov, S., Conrad, D. W., Loew, L., and Hellinga, H. W. (2002) *Protein Sci.* **11,** 2655–2675
11. Brune, M., Corrie, J. E.., and Webb, M. R. (2001) *Biochemistry* **40,** 5087–5094
12. Ebersbach, G., and Gerdes, K. (2005) *Annu. Rev. Genet.* **39,** 453–479
13. van den Ent, F., Møller-Jensen, J., Amos, L. A., Gerdes, K., and Löwe, J. (2002) *EMBO J.* **21,** 6935–6943
14. Garner, E. C., Campbell, C. S., Weibel, D. B., and Mullins, R. D. (2007) *Science* **315,** 1270–1274
15. Popp, D., Narita, A., Oda, T., Fujisawa, T., Matsuo, H., Nitanai, Y., Iwasa, M., Maeda, K., Onishi, H., and Maéda, Y. (2008) *EMBO J.* **27,** 570–579
16. Salje, J., and Löwe, J. (2008) *EMBO J.* **27,** 2230–2238
17. Pace, C. N., Vajdos, F., Fee, L., Grimsley, G., and Gray, T. (1995) *Protein Sci.* **4,** 2411–2423
18. Leatherbarrow, R. J. (2001) *Grafit*, Version 5, Erithacus Software Ltd., Horley, UK
19. Brune, M., Hunter, J. L., Howell, S. A., Martin, S. R., Hazlett, T. L., Corrie, J. E., and Webb, M. R. (1998) *Biochemistry* **37,** 10370–10380
20. Garner, E. C., Campbell, C. S., and Mullins, R. D. (2004) *Science* **306,** 1021–1025
21. Møller-Jensen, J., Jensen, R. B., Löwe, J., and Gerdes, K. (2002) *EMBO J.* **21,** 3119–3127
22. Okoh, M. P., Hunter, J. L., Corrie, J. E., and Webb, M. R. (2006) *Biochemistry* **45,** 14764–14771
23. van den Ent, F., Amos, L. A., and Löwe, J. (2001) *Nature* **413,** 39–44
24. Lara, B., Rico, A. I., Petruzzelli, S., Santona, A., Dumas, J., Biton, J., Vicente, M., Mingorance, J., and Massidda, O. (2005) *Mol. Microbiol.* **55,** 699–711
25. Roeben, A., Kofler, C., Nagy, I., Nickell, S., Hartl, F. U., and Bracher, A. (2006) *J. Mol. Biol.* **358,** 145–156
26. Iordanescu, S., and Bargonetti, J. (1989) *J. Bacteriol.* **171,** 4501–4503
27. Dillingham, M. S., Wigley, D. B., and Webb, M. R. (2000) *Biochemistry* **39,** 205–212
28. Dillingham, M. S., Wigley, D. B., and Webb, M. R. (2002) *Biochemistry* **41,** 643–651
29. Av-Gay, Y., and Everett, M. (2000) *Trends Microbiol.* **8,** 238–244
30. Villarino, A., Duran, R., Wehenkel, A., Fernandez, P., England, P., Brodin, P., Cole, S. T., Zimny-Arndt, U., Jungblut, P. R., Cerveñansky, C., and Alzari, P. M. (2005) *J. Mol. Biol.* **350,** 953–963
31. Nott, T. J., Kelly, G., Stach, L., Li, J., Westcott, S., Patel, D., Hunt, D. M., Howell, S., Buxton, R. S., O'Hare, H. M., and Smerdon, S. J. (2009) *Sci. Signal.* **2,** ra12
32. Takahashi, Y., and Tokumoto, U. (2002) *J. Biol. Chem.* **277,** 28380–28383
33. Johnson, D. C., Dean, D. R., Smith, A. D., and Johnson, M. K. (2005) *Annu. Rev. Biochem.* **74,** 247–281
34. Petrovic, A., Davis, C. T., Rangachari, K., Clough, B., Wilson, R. J., and Eccleston, J. F. (2008) *Protein Sci.* **17,** 1264–1274
35. Eccleston, J. F., Petrovic, A., Davis, C. T., Rangachari, K., and Wilson, R. J. M. (2006) *J. Biol. Chem.* **281,** 8371–8378
36. West, T. G., Hild, G., Siththanandan, V. B., Webb, M. R., Corrie, J. E., and Ferenczi, M. A. (2009) *Biophys. J.* **96,** 3281–3294